Check for updates

Facile synthesis of graphene oxide from graphite rods of recycled batteries by solution plasma exfoliation for removing Pb from water

Nguyen Van Hao,[a] Nguyen Van Dang,*[a] Do Hoang Tung,[b] Pham The Tan,[c] Nguyen Van Tu[d] and Pham Van Trinh ![ORCID] *[de]

We herein present a simple, fast, efficient and environmentally friendly technique to prepare graphene oxide (GO) from graphite rods of recycled batteries by using solution plasma exfoliated techniques at atmospheric pressure. The prepared GO with an average 3 nm-thickness and 1.5 μm-length, having large surface area and high porosity, has been used to remove Pb(II) ions from the water. The obtained results indicated that the adsorption of Pb(II) onto GO depends on pH, contact time, temperature and initial concentration of Pb(II). The maximum adsorption capacity of Pb(II) onto GO determined from the Langmuir model (with a high R^2 value of 0.9913) was 180.1 mg g^{-1} at room temperature. A removal efficiency of ~96.6% was obtained after 40 min. Calculations of thermodynamic parameters ($\Delta G°$, $\Delta H°$ *và* $\Delta S°$) show the adsorption of Pb(II) ions on the GO surface is spontaneous and intrinsically heat-absorbing. The potential mechanism can be suggested here to be the interaction of the $\pi-\pi*$ bonding electrons and Pb(II) as well as the electrostatic attraction between Pb(II) and the oxygen-containing functional groups on GO.

1. Introduction

Toxic metal pollution is a serious environmental problem today. Toxic metal ions are often difficult to biodegrade and easily accumulate in both plants and animals, thus causing danger to humans and organisms.[1–3] Therefore, they are necessary to be removed from wastewater before it goes into the environment. There are many methods to remove toxic metals including chemical reduction, co-precipitation, filtration, ion exchange, ion flotation, adsorption, *etc.* which have been used to treat toxic metal ion-containing wastewater.[4–9] In particular, the adsorption method is considered a more attractive method due to its simple operation, low cost, easy to recycle adsorbents and high efficiency.[10–15] Many previous reports have shown that there are many materials capable of adsorbing toxic metals such as activated carbon, fly ash, sawdust, rice husks, zeolite, iron oxide and manganese.[16–21] However, these adsorbents have a low effective removal of toxic metals due to their low affinity.[22]

Therefore, new materials need to be searched for more effective removal of toxic metals.

In recent years, graphene-based materials have attracted a lot of attention due to their unique properties.[23] In which, graphene oxide (GO) is a type of graphene containing oxygen-rich functional groups such as –OH, –C=O, COOH… on the surface thereby increasing their reactivity and hydrophilic properties. Therefore, GO could be used in many different fields such as materials technology, energy, health and environmental treatment.[24] Up to now, many techniques have been developed for synthesizing GO including mechanical exfoliation, the liquid-phase exfoliation. The preparation of GO from inexpensive graphite powder is a promising method for low-cost and large-scale manufacturing. However, it is well-known that graphite is currently used as an electrode material for most of commercial batteries and thus could become a critical material in the near future. The reuse of the graphite of the recycled batteries could be a potential solution for the future demand of graphite.

Thus, the goal of this work is to prepare GO from the graphite rod of recycled battery by solution plasma exfoliation at atmospheric pressure. The prepared GO having a large surface area and high porosity has been applied for removing Pb(II) ions from the water. The effects of several factors such as pH, contact time, temperature and initial concentration of Pb(II) on the adsorption of GO were also analyzed in detail. Besides, the adsorption kinetics, isothermal and thermodynamic modeling studies were performed to examine the adsorption properties of GO for Pb(II).

[a]Faculty of Physics and Technology, TNU – Thai Nguyen University of Science, Thai Nguyen City, Vietnam. E-mail: dangnv@tnus.edu.vn

[b]Institute of Physics, Vietnam Academy of Science and Technology, 18 Hoang Quoc Viet, Hanoi, Vietnam

[c]Hung Yen University of Technical Education, Khoai Chau, Hung Yen Province, Vietnam

[d]Institute of Materials Science, Vietnam Academy of Science and Technology, 18 Hoang Quoc Viet, Hanoi, Vietnam. E-mail: trinhpv@ims.vast.vn

[e]Graduate University of Science and Technology, Vietnam Academy of Science and Technology, 18 Hoang Quoc Viet, Hanoi, Vietnam

2. Experimental

2.1. Materials

A graphite rod is taken from the recycled battery core (AA SIZE, Panasonics – Malaysia). KOH, $(NH_4)_2SO_4$, NaOH, HCl chemicals were purchased from the Xinyang chemical (China). $Pb(NO_3)_2$ in analytical adsorption is supplied by Sigma Aldrich. The experimental solution is double distilled water.

2.2. GO synthesis experiments

The solution plasma exfoliated processing of the synthesis of GO using the graphite rod of recycled battery is shown in Fig. 1. The system consists of a 150 ml beaker used as a reaction vessel, two electrodes are placed parallel and deeply immersed in the electrolyte solution. The positive electrode is a graphite rod collected from old AA batteries with a diameter of 5.0 mm and a length of 50 mm. The negative electrode is a pure platinum rod (99.9%). The electrolyte solution is a mixture of 500 ml of 0.5 mM KOH and 0.2 mM $(NH_4)_2SO_4$. The two electrodes are connected by a home-made DC high voltage supply. It is a modulated DC power supplier with an average voltage of 2.45 kV and a current of 22.4 mA. Plasma is created between the two electrodes at a distance of 0.2 mm (Fig. 1a). After the plasma process, the obtained solution is filtered and washed with PVDF film (0.2 µm) to remove impurities and organic compounds from the battery core. Finally, the samples were dried at 60 °C in a vacuum for 14 hours.

2.3. Characterization

Samples are characterized by field emission scanning electron microscopy (FESEM, Hitachi S4800), atomic force microscopy (AFM, PARK XN100), X-ray diffractometer (Miniflex Rigaku), absorption spectra (UV-Vis, Jasco-V770), Raman spectroscopy by using 532 nm wavelength at room temperature (XploRA, Horiba Jobin-Yvon), and spectrum Fourier transform infrared (FTIR) with 4 cm^{-1} resolutions (Spectrum Two, PerkinElmer, USA). The BET specific surface areas (S_{BET}) of GO were determined by N_2 adsorption/desorption isotherms at 77 K (BET, Builder, SSA-4300).

2.4. Batch adsorption experiments

The adsorption efficiency of GO for Pb(II) was evaluated and investigated *via* parameters including contact time (5–180 minutes), pH (3–9), contact temperature (293–313 K) and initial concentration (60–200 mg L^{-1}). A Pb(II) solution of 1000 mg L^{-1} was prepared using $Pb(NO_3)_2$ dispersed in distilled water. The initial pH of Pb(II) solution is adjusted from 3 to 9 using NaOH and HCl solutions. The pH of the solution is measured by a pH meter (PHS-3C, Hinotek, China).

The Pb(II) adsorption experiments were performed by adding 50 mg of GO to a 100 ml conical glass flask containing 50 ml of Pb(II) solution and shaking with a shaker (model: MaxQ 4000 Benchtop, Thermo Scientific, USA) over time (at a speed of 120 rpm). The solution is then filtered, centrifuged to separate the supernatant. The Pb(II) concentration at various contact time was analyzed using AAS (Hitachi, Japan). Adsorption efficiency R_e (%) and adsorption capacity q_e are determined by the following equation:

$$R_e(\%) = \frac{(C_0 - C_e) \times 100\%}{C_0} \qquad (1)$$

$$q_e = \frac{(C_0 - C_e)V}{m} \qquad (2)$$

where C_0 is the initial concentration of Pb(II) (mg L^{-1}), C_e is the equilibrium concentration of Pb(II) after adsorption (mg L^{-1}), q_e is the equilibrium adsorption capacity of Pb(II) (mg g^{-1}), m is the mass of GO adsorbent (g), and V is the volume of Pb(II) solution (L).

3. Results and discussions

3.1. The characteristics of GO

Fig. 2a and b shows the morphology of GO produced by plasma technology in solution from the recycled battery core. The average thickness and diameter of the prepared GO were determined by the statically counting of about more than 100 sheets from AFM images as shown in Fig. 2c and d. The results
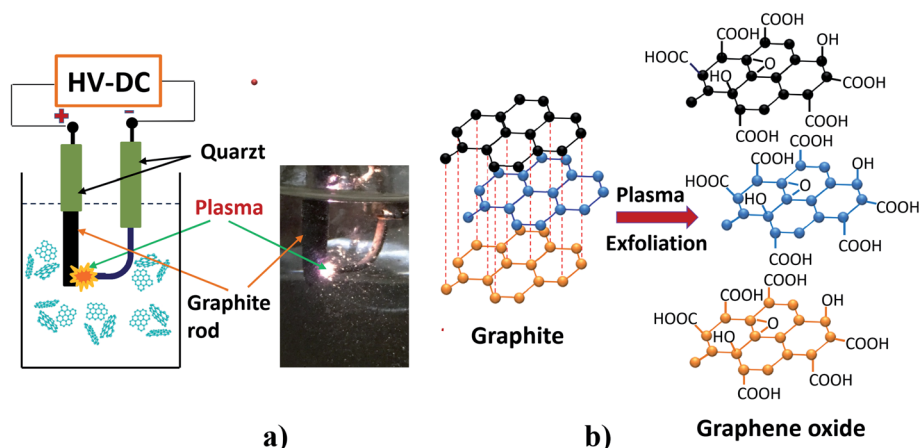

Fig. 1 The solution plasma exfoliated processing of graphene oxide synthesis using graphite rod of recycled battery core (a) experimental setup and (b) possible mechanism.
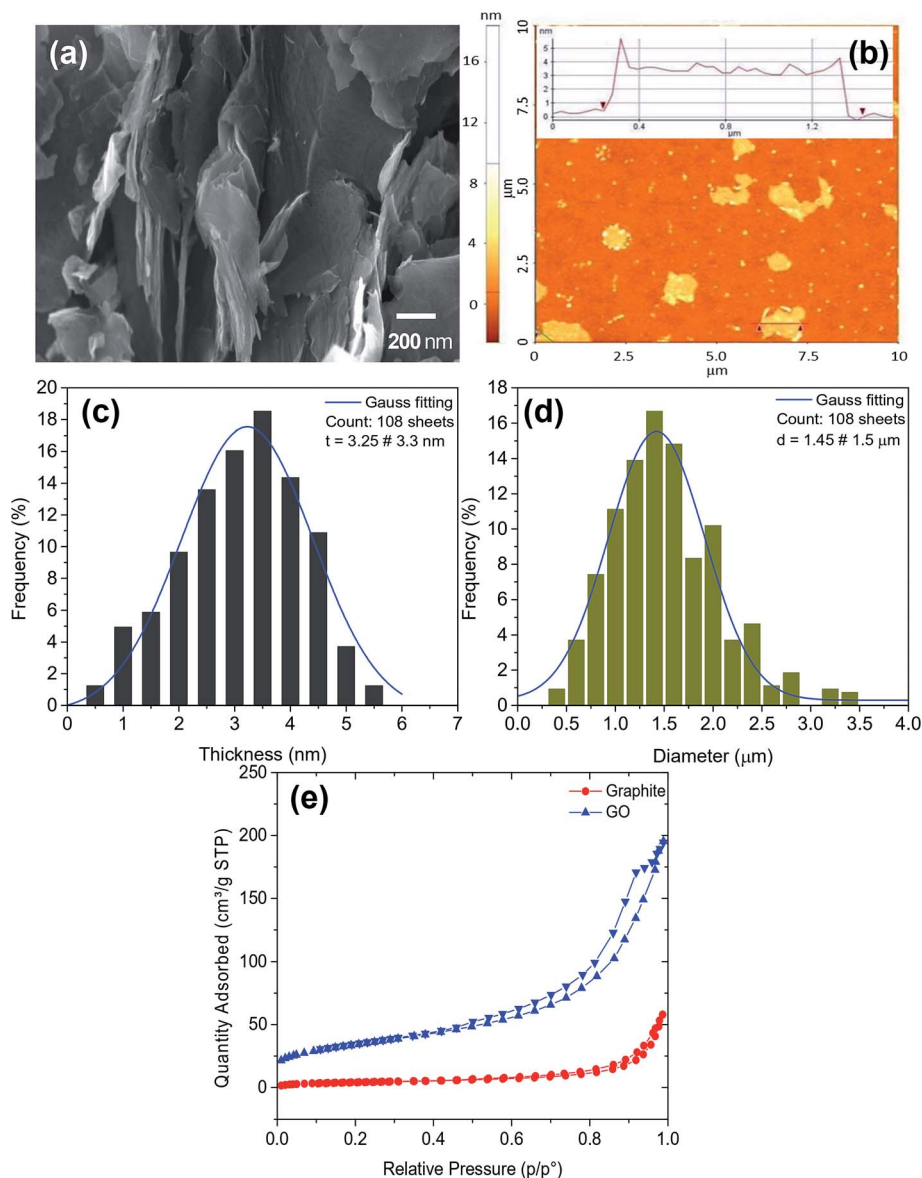
Fig. 2 (a) SEM and (b) AFM images of GO, the statistical distribution of thickness and diameter (c and d) and (e) N_2 adsorption/desorption isotherms exfoliation of graphite and GO at 77 K.

Table 1 Surface characteristics of graphite and GO

Materials	S_{BET} $(m^2\ g^{-1})$	Average pore diameter (nm)	Total pore volume $(cm^3\ g^{-1})$
Graphite	15.78	9.56	0.074
GO	128.37	19.73	0.36

indicated that the average thickness of nanosheet size of 3.3 nm corresponds to the number of layers from 8–10 layers, the average diameter of about 1.5 μm. Fig. 2e presents the N_2 adsorption/desorption isotherm curves at 77 K of graphite rod and GO. The results show BET surface areas and the total pore volume of graphite and GO are 15.78 $m^2\ g^{-1}$, 0.074 $cm^3\ g^{-1}$ and 128.37 $m^2\ g^{-1}$, 0.36 $cm^3\ g^{-1}$, respectively. The characteristics of porous structure and BET surface area of graphite and GO are

detailed in Table 1, it demonstrated that the surface area of GO significantly increases compared to graphite.

Fig. 3a shows the UV-Vis spectra of aqueous graphite, GO and GO dispersion after Pb(II) adsorption process. The results showed that the UV-Vis spectra of GO have two observed features, the first is a shoulder at ∼310 nm, attributed to the plasmon peak related to the n–π* transition due to the presence of the oxygen-containing functional groups and the second feature is a peak appearing near 235 nm are related to the plasmon peak due to the transition of the π–π* electron in C–C the aromatic ring bond of the graphene layers.[25–28] While the UV-Vis spectra of graphite show only one wide band with a slight transition peak of ∼275 nm as a characteristic of this material.[28–33] It is interesting noted that the absorption spectrum of GO after Pb(II) adsorption has a significant change both in curve form and in spectral intensity, the first
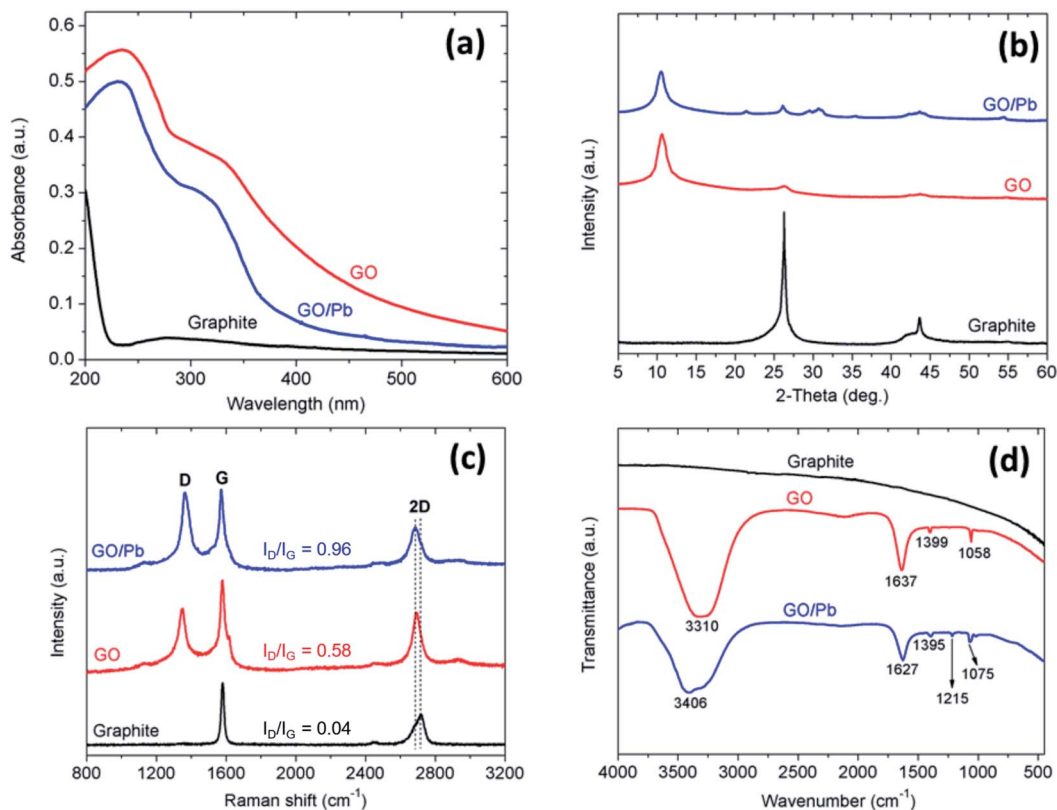
Fig. 3 (a) UV-Vis spectra (b) XRD patterns, (c) Raman spectra and (d) FTIR spectra of graphite rod, GO and GO after adsorption of Pb(II).

is the plasmon peak at 235 nm is shifted to 231 nm, while the shoulder at about 310 nm is shifted to the position 305 nm with a steeper slope. This result shows that Pb(II) ions were adsorbed on the surface of GO. As a result, the optical absorption of GO is dominated by the π–π* plasmon peak near 230 nm, this plasmon peak depends on the effects related to the nanometer-scale sp^2 clusters and the C=C, C=O and C–O bonds, respectively, with deconvoluted peaks at the binding energy ranges of 284.8–285.0, 288.0–288.9 and 286.0–286.9 eV.[34–40]

Fig. 3b shows the XRD patterns of graphite and GO. The results show that in addition to the peak with strong intensity at the angle of $2\theta = 26.24°$ (002), some peaks appearing at 43.24° (100) and 54.92° (004) which are typical peaks of graphite. As for GO, besides typical peaks of graphite, a new peak with high intensity appears at $2\theta = 10.71°$. It is noted that the typical peak of graphite (002) is slightly shifted to 26.34° with a lower intensity. This is attributed to the graphite do not completely oxidize during the plasma process and still retain part of its graphite structure. The d-distance of GO was determined to be 0.8745 nm, implying that some oxygen functional groups were attached to the surface of graphene layers. When comparing the XRD patterns of GO before and after Pb(II) adsorption, the intensity of the peak at $2\theta = 10.71°$ is decreased and the peak position is slightly shifted. In addition, the presence of new peaks at $2\theta =$ 21.46°, 26.11°, 29.53°, 30.70°, 35.50°, 42.33°, 43.65°, 54.42° indicating that Pb(II) was adsorbed on the surface of GO.[41,42]

Fig. 3c shows the Raman spectrum of graphite, GO and GO/Pb. Raman spectra of graphite showed the presence of D-band

at 1350 cm^{-1} with very low intensity representing defects related to vacancy and grain boundaries and G-band (graphite) at 1579 cm^{-1} with high intensity relative to sp^2 carbon atoms due to scattering of the E$_{2g}$ phonons.[43,44] The 2D-band at 2717 cm^{-1} with relatively high intensity is attributed to a two-phonon double resonance.[45,46] For GO, the Raman spectra all showed a slight shift in the bands (D-band at 1350.2 cm^{-1}, G-band at 1580 cm^{-1} and 2D-band at 2691 cm^{-1}). The I_D/I_G ratios of graphite and GO were 0.04 and 0.58, respectively. The increase in the I_D/I_G ratio can be explained by oxidation of graphite during the plasma exfoliation process in solution and thereby also confirming the degree of surface functionalization of GO (e.g., introduces a few of containing oxygen functional groups).[46] In addition, the 2D band of GO has been slightly shifted to low frequencies with a significantly higher intensity than graphite, which indicated the formation of the graphene sheets from the graphite rod during the plasma generation process.[47,48] After Pb(II) adsorption, the D band and G band are shifted to 1363 and 1572 cm^{-1}, respectively and the I_D/I_G ratio increased up to 0.96. The peak shifts and the increase of the I_D/I_G ratio are attributed to the adsorption of Pb(II) on the surface of GO.[42]

Fig. 3d shows the FTIR spectrum of graphite, GO and GO after adsorption of Pb(II). For graphite, the FTIR spectrum is a wide range covering the entire spectrum without any peak containing the functional groups such as C=O, C–O, COO–.[49] While the FTIR spectrum of GO is prepared by plasma process in a solution from graphite rods taken from the recycled battery core showing signs of oxygen-derived species, the functional

groups are obvious in the structure, such as a strong band at 3310 cm^{-1} attributable to the stretch oscillation of the OH group, a narrower peak at 1637 cm^{-1} related to the stretching oscillations from carbonyl and carboxylic groups (C=O), the peak that appears at 1399 cm^{-1} corresponds to the stretching oscillations of COO$^-$ (ref. 50) and the peak at 1058 cm^{-1} indicates the stretching oscillations associated with the C–O group on the surface of the GO.[51] This indicates that functional groups containing oxygen already exist on the surface of the GO plates. Compared with the FTIR spectrum of GO before adsorption, the peak intensity at 3310 cm^{-1} and 1637 cm^{-1} has a slight decrease and shift after Pb(II) adsorption. This is explained by the interaction of Pb(II) ions with oxygen-containing functional groups on the surface of GO. The peak at 1058 cm^{-1} also has decreased intensity and the red shift. This is probably due to the electron delocalization in the surface structure of GO when Pb(II) is adsorbed, causing the density to decrease and the bond length increasing, leading to a red shift.[42,52] In addition, a new peak at 1215 cm^{-1} appeared in the spectrum, attributed to the stretching vibration of C=C.

3.2. Removal Pb(II) in water using GO

The adsorption is a process that depends on many factors such as the pH of the solution, temperature, the initial concentration of the toxic metal and the properties of the adsorbent.

PH is a parameter that greatly influences the adsorption capacity of the adsorbent. To investigate the effect of PH on the removal of Pb(II) ions, the pH of the solution was changed in the range from 3 to 9 at the fixed initial concentration of Pb(II) of 100 mg L^{-1}. Fig. 4a shows the effect of pH on the adsorption capacity of GO for Pb(II). The results showed that adsorption capacity increased when the pH increased from 3 to 6 and reached a stable value at pH about 6–7 and then decreased slightly. The increase in adsorption capacity can be explained by the competition between H$^+$ and Pb^{2+} ions decreased on GO or due to the reduction of electrostatic repulsion between GO and Pb^{2+} surfaces because of positive charge on the surface decreases,[53,54] therefore it is stable at pH values of 6–7. The reduced adsorption at pH > 7 may be due to the precipitation of Pb(II) on the GO surface.[55,56] As a result, a pH value of 6 was chosen for the subsequent experiments.

Fig. 4b shows the effect of contact time on the adsorption for Pb(II) of GO. Experimental conditions at pH 6, initial concentration of Pb(II) 100 mg l^{-1}, the GO concentration is 1 mg ml^{-1} in 50 ml of solution at room temperature and the contact time is changed from 5 to 180 minutes. The obtained results showed that, in the first 20 minutes, the adsorption capacity increased rapidly. As increasing the adsorption time, the adsorption increased to a stable value of about 40 minutes and this is considered to be the adsorption equilibrium time. Fig. 4c shows the effect of the initial concentration of Pb(II) on the adsorption of GO. The results indicated that, when the initial concentration of Pb(II) increased from 60 mg l^{-1} to 200 mg l^{-1}, the adsorption capacity increased accordingly, from 59.5 mg g^{-1} to 113.7 mg g^{-1}. This result can be explained by the fact that under optimal pH conditions, the surface of GO will contain H$^+$ ions that help elevate ions interactions with the functional groups on the GO
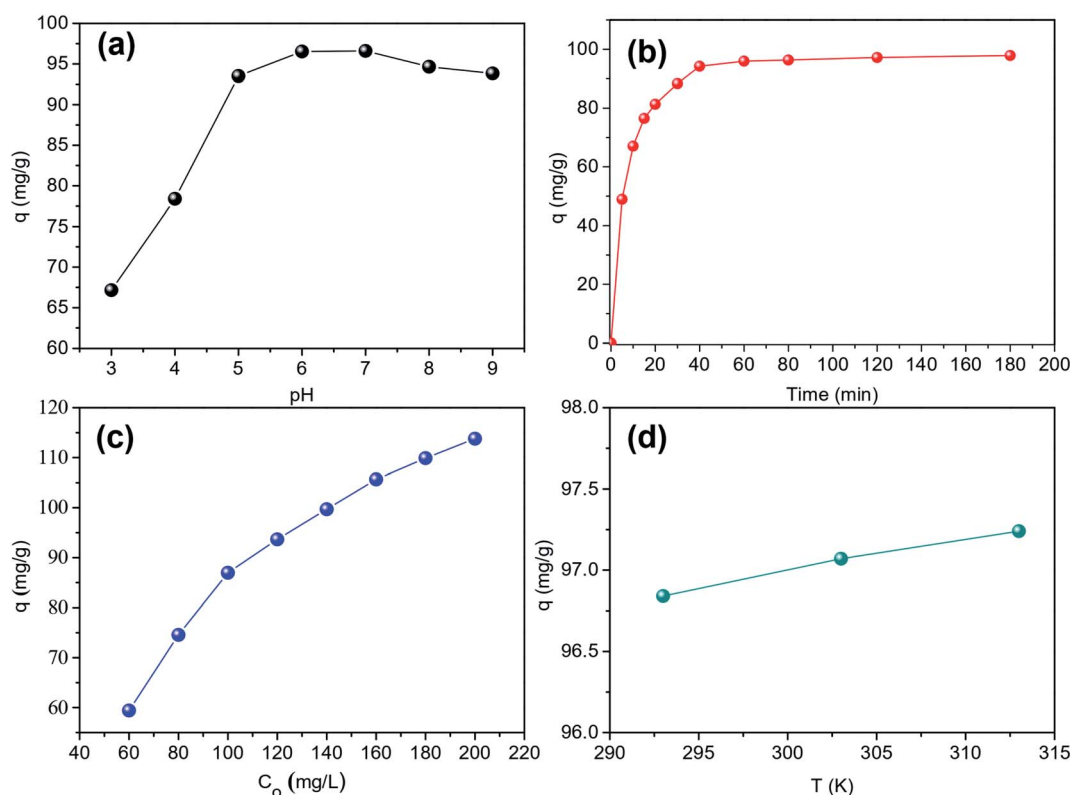

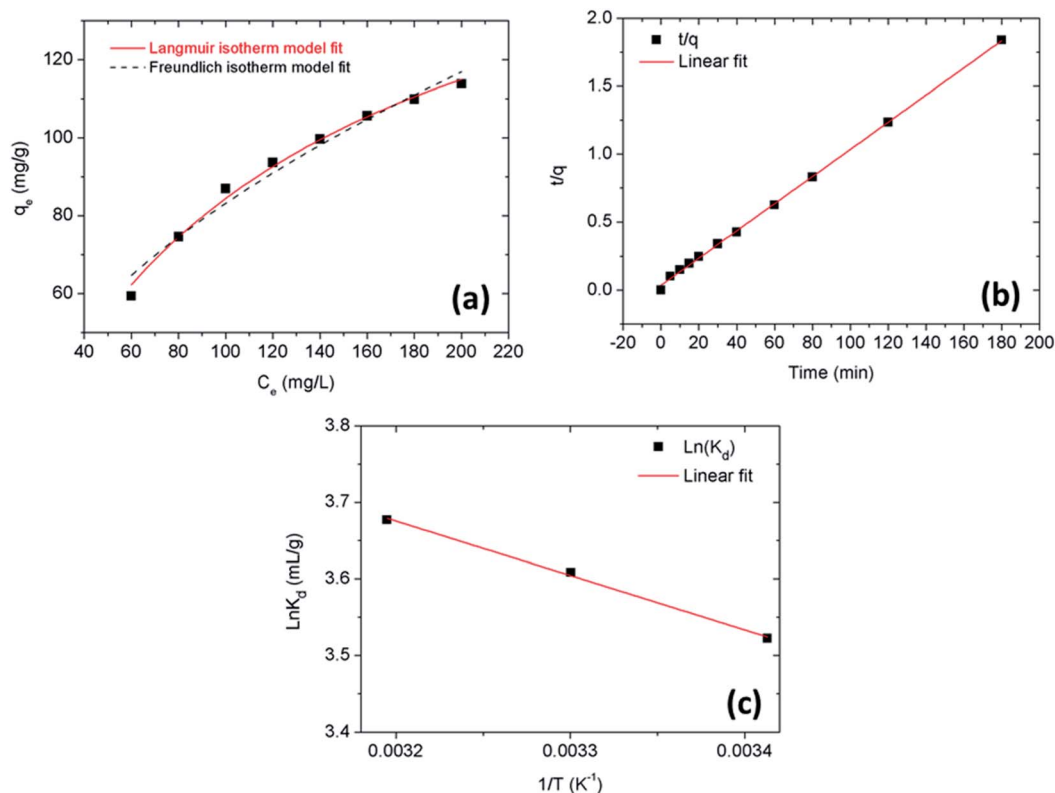Fig. 4 Effect of (a) pH, (b) contact time, (c) initial concentration and (d) temperature on the Pb(II) adsorption of GO.

Fig. 5 (a) Linear fit curve of the second-order Pseudo adsorption kinetic model data, (b) adsorption isotherms of Pb(II) onto the GO (1 mg ml^{-1}) at different initial concentrations (60–200 mg l^{-1}) after 60 min and (c) linear plot of ln K_d vs. 1/T for Pb(II) adsorption onto GO at $T = 293, 303, 313$ K.

surface or because GO has highly porous, thus it could adsorb more Pb(II) ions at higher concentrations.[56,57]

The effect of temperature on Pb(II) adsorption by GO was performed by changing the temperature in the range of 293–313 K, during 60 minutes contact time and pH 6 and as illustrated in Fig. 4d. The results showed that, when the temperature increased from 293 to 313 K, the adsorption capacity increased slightly from 96.84 to 97.24 mg g^{-1}. This indicated that the Pb(II) adsorption process is an endothermic process because it is possible that the porosity and total pore volume of the adsorbent increase, leading to increases in the number of available active sites on the adsorbent as the temperature increases, however, it does not increase much. The same tendency has been obtained in some previous studies.[56–62]

To better understand the effect of contact time onto the Pb(II) adsorption process, the first-order second Pseudo (eqn (3)) and second-order Pseudo models (eqn (4)) were used to fit data:

$$q_t = q_e(1 - e^{-k_1 t}) \quad (3)$$

$$q_t = \frac{q_e^2 k_2 t}{1 + q_e k_2 t} \quad (4)$$

where q_e and q_t are equilibrium adsorption and at time t for Pb(II) (mg g^{-1}) of GO, respectively and k_1, k_2 are the rate constants of first-order Pseudo kinetic adsorption and second-order Pseudo adsorption kinetic models, respectively.

Fig. 5a shows the linear fit curve of the second-order Pseudo adsorption kinetic model data. The calculated results show that the adsorption kinetics of Pb(II) on GO fits well with both kinetic models. Table 2 shows the parameters obtained from fit data following the first-order Pseudo and second-order Pseudo models. As a result, the value of R^2 for the second-order Pseudo kinetic model (0.9983) is higher than the first-order Pseudo kinetic model (0.9871), which shows the action time in the adsorption process is mainly based on chemical adsorption. These results are consistent with the previous publication.[42,57,63]

To study precisely the equilibrium relationship between GO and Pb(II), the two most common adsorption isotherm models,

Table 2 Kinetic parameters for Pb(II) adsorption models

Kinetic models	Pseudo-first-order model			Pseudo-second-order model		
Parameters	R^2	q_e (mg g^{-1})	k_1 (min^{-1})	R^2	q_e (mg g^{-1})	k_2 (g mg^{-1} min^{-1})
	0.9871	94.98	0.1197	0.9983	102.98	0.0018

Table 3 Isothermal parameters of Pb(II) adsorption

Isotherm models	Langmuir			Freundlich		
Parameters	R^2	q_m (mg g^{-1})	k_L (L mg^{-1})	R^2	$1/n$	k_F (g mg^{-1})
	0.9913	180.13	0.008	0.9692	0.4908	8.673

the Langmuir and Freundlich isotherm models were utilized to describe the Pb(II) adsorption onto GO. The Langmuir and Freundlich isotherm models are expressed as.[64,65]

$$q_e = \frac{q_m k_L C_e}{1 + k_L C_e} \quad (5)$$

$$q_e = k_F C_e^{1/n} \quad (6)$$

where q_e (mg g^{-1}) is the equilibrium adsorption capacity of Pb(II) onto GO, q_m (mg g^{-1}) is the maximum adsorption capacity of Pb(II) onto GO, C_e (mg L^{-1}) is the equilibrium concentration of Pb(II), k_L is the Langmuir constant, k_F and $1/n$ are Freundlich constants. Fig. 5b presents the adsorption isotherms of Pb(II) on GO at different initial concentrations. The isothermal parameters of those models were given in Table 3. The fit result of the model shows that the value of R^2 of the Langmuir model is higher than that of the Freundlich model, which indicates the suitability in Langmuir isotherms of GO for Pb(II). The adsorption capacity of GO calculated as 180.1 mg g^{-1} is quite high compared to the list of other adsorbents (Table 4).

Thermodynamic parameters including Gibbs free energy $\Delta G°$, entropy change $\Delta S°$, enthalpy change $\Delta H°$ are investigated through adsorption of Pb(II) onto GO at different temperatures and is described as by the following equations:[71]

$$\ln(K_d) = \frac{\Delta S°}{R} - \frac{\Delta H°}{RT} \quad (7)$$

$$K_d = \frac{q_e}{C_e} \quad (8)$$

$$\Delta G° = -RT \ln(K_d) \quad (9)$$

$$\Delta G° = \Delta H° - T\Delta S° \quad (10)$$

where T is the temperature (K), R is the gas constant (8.314 J mol^{-1} K^{-1}), K_d is the adsorption equilibrium coefficient, $\Delta S°$ and $\Delta H°$ are determined by the intercept and slope of the linear fitting of $\ln(K_d)$ to $1/T$ plot, respectively.

The thermodynamic parameters determined from Fig. 5c are presented in Table 5. Positive $\Delta H°$ values indicate the adsorption of Pb(II) onto GO as an endothermic process. This result is in good agreement with the previous discussion. Moreover, the free energy change Gibbs $\Delta G° < 0$ and when the environment temperature increases, the value of $\Delta G°$ decreases, which shows the absorption of Pb(II) on the GO surface is more favorable when the temperature increases, this is because at higher temperatures the ions are more prone to dehydration. With the value $\Delta H° = 5.9$ kJ mol^{-1} < 40 kJ mol^{-1}, so this is a physisorption process.[63,71] At the same time, the value $\Delta S° > 0$ also confirmed that the adsorption was spontaneous with high affinity.

To investigate the recyclability of the GO material, the regeneration experiment was repeated 7 times. Fig. 6 shows the adsorption efficiency of GO on Pb(II) when using regenerated GO for 7 repeated uses. The regeneration of the GO adsorbent was evaluated for up to 7 consecutive cycles and after each cycle, the adsorption efficiency was reduced. However, after 6 cycles, the Pb(II) adsorption efficiency still reached 72.94%. This can be explained by a variation in the surface activity position of GO. This is because of the incomplete separation of the Pb(II) ions involved in ion-exchange interactions. Besides, another possible reason for performance degradation per cycle could be partial erosion of the GO surface in a strongly acidic environment. This obtained result is consistent with previous studies on Pb(II) adsorption[42,72–74] and shows the recyclability and stability of the prepared materials.

3.3. The possible mechanisms of adsorption

Based on the analysis results of UV-Vis absorption spectra, FTIR, Raman spectra and XRD of GO before and after Pb(II) adsorption as well as the discussion of the results above, Pb(II) removal mechanism by GO can be proposed as in Fig. 7. From the optical absorption analysis of Pb(II)-loaded GO (Fig. 3a), it

Table 4 q_{max} of Pb(II) by different adsorbents

Adsorbents	q_{max} (mg g^{-1})	Year of publication	Ref.
GO	81.3	2019	42
Nickel ferrite–rGO	121.6	2018	66
SV–rGO	95	2019	67
CNTs	38.76	2011	70
GO	111	2016	56
GO-SH1	142.8	2016	56
GO-SH2	200	2016	56
GOA	158.7	2016	68
GO–Zr–P	384.6	2016	65
GO/chitosan	99	2011	69
GO	180.1	—	This work

Table 5 Thermodynamic parameters of Pb(II) adsorption onto GO

T (K)	$\Delta G°$ (kJ mol^{-1})	$\Delta S°$ (J mol^{-1} K^{-1})	$\Delta H°$ (kJ mol^{-1})
293	−8.58	49.45	5.90
303	−9.08		
313	−9.57		
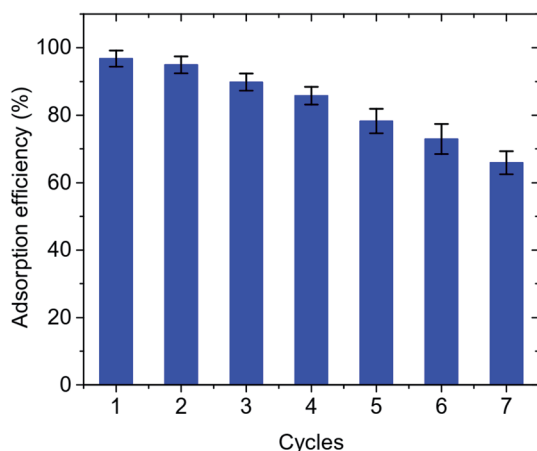
Fig. 6 Regeneration experiment for Pb(II) adsorption by GO.

can be seen that the change of plasmon absorption peak is near 230 nm compared to the peak at 235 nm of GO, this indicates that there is Pb(II) attachment to the surface of GO. This is due to the complexation interaction of Pb(II) ions and the π–π^* bonding electrons involving bonds such as C=C (at energy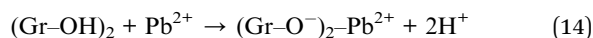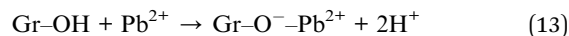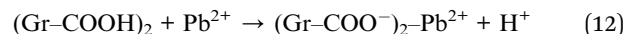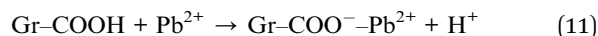 range 284.8–285.0 eV), C=O (in the range energy 288.0–288.9 eV), O–C=O (at the energy range 286.0–289.6 eV), –COOH (at the energy range 530–531.5 eV) and –C=O (at the energy range 531.8–532.2 eV).[75–78] Fig. 3d illustrates the FTIR spectra of the loaded Pb(II) GO after adsorption showing peaks with a decrease in intensity and transition from 3310 cm^{-1} to 3406 cm^{-1}, from 1637 cm^{-1} to 1627 cm^{-1}, which could due to the complexation of Pb(II) with the –OH group and the –C=O group in carboxylic acid, respectively.[79,80] The peak shift to 1075 cm^{-1} could be attributable to hydroxyl group re-formation on lead oxide or to the C–O stretching vibration of –COOH due to the hydroxyl group complexation of Pb(II) with sites.[79,81] The appearance of a new peak at 1215 cm^{-1}, is attributed to the stretching vibration of C=C group in the nanometer-scale sp^2 carbon skeletal lattice. Previous studies of Pb(II) binding with oxygen-containing functional groups on the surface of oxidized poly-walled CNTs, GO and rGO have been reported[42,79,82,83] and the results from spectral analysis UV-Vis, FTIR, the surface complexing reactions of GO can be represented by the following equations:[83]

$$Gr-COOH + Pb^{2+} \rightarrow Gr-COO^--Pb^{2+} + H^+ \quad (11)$$

$$(Gr-COOH)_2 + Pb^{2+} \rightarrow (Gr-COO^-)_2-Pb^{2+} + H^+ \quad (12)$$

$$Gr-OH + Pb^{2+} \rightarrow Gr-O^--Pb^{2+} + 2H^+ \quad (13)$$

$$(Gr-OH)_2 + Pb^{2+} \rightarrow (Gr-O^-)_2-Pb^{2+} + 2H^+ \quad (14)$$

$$Gr-COOH + Pb^{2+} + -OH \rightarrow Gr-COO-PbO- + 2H^+ \quad (15)$$
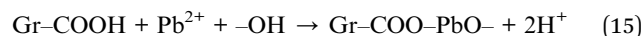
The schematic representation of the proposed Pb(II) adsorption at positions on the surface of the GO plate as shown in Fig. 7. The Pb(II) is mainly attached to the positions of the hydroxyl and carbonyl groups (as given in eqn (11)–(15)). This can be considered as an approximate representation of the adsorption capacity of Pb(II) on the surface of GO.[79]

4. Conclusions

We have investigated the method basing on a plasma exfoliated process to prepare GO from a recycled battery core in solution was performed. This is considered to be a simple, inexpensive, novel and environmentally friendly technique. The prepared GO has an average thickness of 3.5 nm and a length of 1.5 μm. The properties of GO are suitable for the adsorption of toxic metals. Experimental results have demonstrated that the adsorption capacity of GO for Pb(II) can reach a maximum value of 180.1 mg g^{-1} at room temperature. Studies of isotherms and adsorption kinetic models have shown that adsorption of GO onto Pb(II) fits well with the Langmuir model. Calculations of thermodynamic parameters ($\Delta G°$, $\Delta H°$, và $\Delta S°$) show that the adsorption of Pb(II) ions on the GO surface is spontaneous and intrinsically heat-
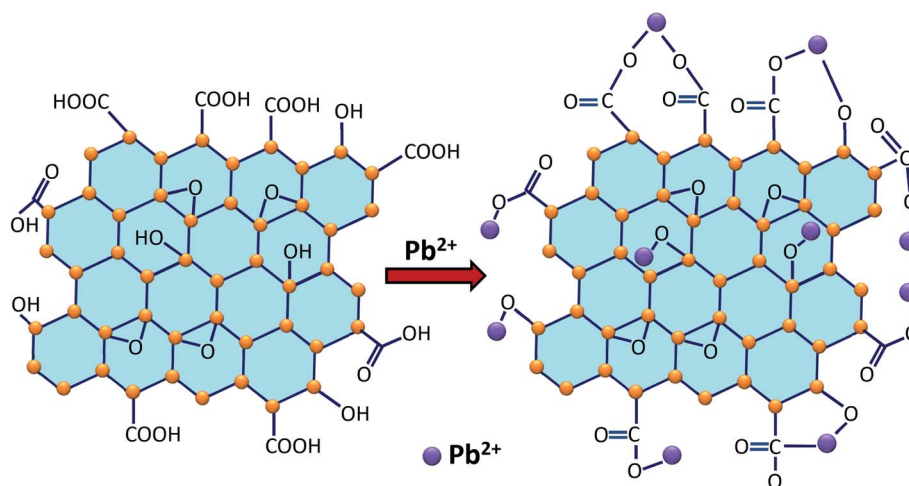

Fig. 7 Possible mechanism for Pb(II) adsorption onto GO.

absorbed. The main Pb(II) adsorption mechanism of GO is the formation of complexation of Pb(II) in the π–π^* bond electrons and the electrostatic interaction between Pb(II) ions and oxygen-containing functional groups are also dominant mechanisms for GO. All these properties make the solution plasma exfoliated GO as a new carbon material and attract a lot of attention, a promising adsorbent for many environmental treatment applications with a high recyclability and efficiency removal contaminants in aqueous solution.

Conflicts of interest

The authors declare no possible conflict of interests.

Acknowledgements

References

1 B. Volesky, Detoxification of metal-bearing effluents: Biosorption for the next century, *Hydrometallurgy*, 2001, **59**, 203–216.

2 Y. Zhang, L. Yan, W. Xu, X. Guo, L. Cui, L. Gao, Q. Wei and B. Du, Adsorption of Pb(II) and Hg(II) from aqueous solution using magnetic $CoFe_2O_4$-reduced graphene oxide, *J. Mol. Liq.*, 2014, **191**, 177–182.

3 P. Kavcar, A. Sofuoglu and S. C. Sofuoglu, A health risk assessment for exposure to trace metals *via* drinking water ingestion pathway, *Int. J. Hyg. Environ. Health*, 2009, **212**, 216–227.

4 S. Babel and T. A. Kurniawan, Low-cost adsorbents for heavy metals uptake from contaminated water: A review, *J. Hazard. Mater.*, 2003, **97**, 219–243.

5 Z. Q. Wang, A. G. Wu, L. C. Ciacchi and G. Wei, Recent advances in nanoporous membranes for water purification, *Nanomaterials*, 2018, **8**, 65.

6 S. Cataldo, G. Lazzara, M. Massaro, N. Muratore, A. Pettignano and S. Riela, Functionalized halloysite nanotubes for enhanced removal of lead(II) ions from aqueous solutions, *Appl. Clay Sci.*, 2018, **156**, 87–95.

7 M. Hepel, X. M. Zhang, R. Stephenson and S. Perkins, Use of electrochemical quartz crystal microbalance technique to track electrochemically assisted removal of heavy metals from aqueous solutions by cation-exchange composite polypyrrole-modified electrodes, *Microchem. J.*, 1997, **56**, 79–92.

8 K. K. Bhatluri, M. S. Manna, A. K. Ghoshal and P. Saha, Supported liquid membrane based removal of lead(II) and cadmium(II) from mixed feed: Conversion to solid waste by precipitation, *J. Hazard. Mater.*, 2015, **299**, 504–512.

9 S. Yan, Y. Li, F. Xie, J. Wu, X. Jia, Y. Jin, H. Song and Z. Zhang, Environmentally Safe and Porous MS@TiO2@PPy Monoliths with Superior Visible-Light Photocatalytic Properties for Rapid Oil–Water Separation and Water Purification, *ACS Sustainable Chem. Eng.*, 2020, **8**, 5347–5359.

10 X. J. Liu, H. Q. Li, X. Y. Lin, H. Y. Liu and G. H. Gao, Synthesis of siloxane-modified melamine–formaldehyde microsphere and its heavy metal ions adsorption by coordination effects, *Colloids Surf., A*, 2015, **482**, 491–499.

11 S. J. Olusegun, G. L. S. Rodrigues, E. T. F. Freitas, L. R. S. Lara, W. R. Rocha and N. D. S. Mohallem, Sequestrating anionic and cationic dyes from wastewater using spray dried biopolymeric magnetic composite: Experimental and theoretical studies, *J. Hazard. Mater.*, 2019, **380**, 120872.

12 N. Minju, G. Jobin, S. Savithri and S. Ananthakumar, Doublesilicate derived hybrid foams for high-capacity adsorption of textile dye effluent: statistical optimization and adsorption studies, *Langmuir*, 2019, **35**, 9382–9395.

13 P. Shao, L. Ding, J. Luo, Y. Luo, D. You, Q. Zhang and X. Luo, Lattice-defect-enhanced adsorption of arsenic on zirconia nanospheres: a combined experimental and theoretical study, *ACS Appl. Mater. Interfaces*, 2019, **11**, 29736–29745.

14 X. Yin, P. Shao, L. Ding, Y. Xi, K. Zhang, L. Yang, H. Shi and X. Luo, Protonation of rhodanine polymers for enhancing the capture and recovery of Ag+ from highly acidic wastewater, *Environ. Sci.: Nano*, 2019, **6**, 3307–3315.

15 P. Shao, D. Liang, L. Yang, H. Shi, Z. Xiong, L. Ding, X. Yin, K. Zhang and X. Luo, Evaluating the adsorptivity of organo-functionalized silica nanoparticles towards heavy metals: Quantitative comparison and mechanistic insight, *J. Hazard. Mater.*, 2020, **387**, 121676.

16 K. B. Payne and T. M. Abdel-Fattah, *J. Environ. Sci. Health, Part A: Toxic/Hazard. Subst. Environ. Eng.*, 2004, **39**, 2275–2291.

17 G. Gupta and N. Torres, *J. Hazard. Mater.*, 1998, **57**, 243–248.

18 D. Lee and H. Moon, *Korean J. Chem. Eng.*, 2001, **18**, 247–256.

19 T. G. Chuah, A. Jumasiah, I. Azni, S. Katayon and S. Y. Thomas Choong, *Desalination*, 2005, **175**, 305–316.

20 R. R. Gadde and H. A. Laitinen, *Anal. Chem.*, 1974, **46**, 2022–2026.

21 L. Joseph, B.-M. Jun, J. R. V. Flora, C. M. Park and Y. Yoon, Removal of heavy metals from water sources in the developing world using low-cost materials, *Chemosphere*, 2019, **229**, 142e159.

22 Y. L. F. Musico, C. M. Santos, M. L. P. Dalida and D. F. Rodrigues, Improved removal of lead(II) from water using a polymer-based graphene oxide nanocomposite, *J. Mater. Chem. A*, 2013, **1**, 3789–3796.

23 R. Tian, X. Jia, Y. Jin, Y. Li and H. Song, Large-scale, green, and high-efficiency exfoliation and noncovalent functionalization of fluorinated graphene by ionic liquid crystal, *Chem. Eng. J.*, 2020, **395**, 125104.

24 X.-M. Huang, Li-Z. Liu, Si Zhou and Ji-J. Zhao, Physical properties and device applications of graphene oxide, *Front. Phys.*, 2020, **15**, 33301.

25 M. J. Fernández-Merino, L. Guardia, J. I. Paredes, S. Villar-Rodil, P. Solís-Fernández, A. Martínez-Alonso and J. M. D. Tascón, Vitamin C is an ideal substitute for

hydrazine in the reduction of graphene oxide suspensions, *J. Phys. Chem. C*, 2010, **114**, 6426–6432.

26 D. Li, M. B. Müller, S. Gilje, R. B. Kaner and G. G. Wallace, Processable aqueous dispersions of graphene nanosheets, *Nat. Nanotechnol.*, 2008, **3**, 101–105.

27 D. W. Lee, V. L. De Los Santos, J. W. Seo, L. L. Felix, D. A. Bustamante, J. M. Cole and C. H. Barnes, The structure of graphite oxide: Investigation of its surface chemical groups, *J. Phys. Chem. B*, 2010, **114**, 5723–5728.

28 C. A. Guerrero-Fajardo, L. Giraldo and J. C. Moreno-Piraján, Preparation and Characterization of Graphene Oxide for Pb(II) and Zn(II) Ions Adsorption from Aqueous Solution: Experimental, Thermodynamic and Kinetic Study, *Nanomaterials*, 2020, **10**, 1022.

29 N. Hu, L. Meng, R. Gao, Y. Wang, J. Chai, Z. Yang, E. S. W. Kong and Y. Zhang, A facile route for the large scale fabrication of graphene oxide papers and their mechanical enhancement by cross-linking with glutaraldehyde, *Nano-Micro Lett.*, 2011, **3**, 215–222.

30 M. Muniyalakshmi, K. Sethuraman and D. Silambarasan, Synthesis and characterization of graphene oxide nanosheets, *Mater. Today: Proc.*, 2020, **21**, 408–410.

31 K. Awasthi, D. P. Singh and S. Singh, Attachment of biomolecules (protein and DNA) to amino-functionalized carbon nanotubes, *New Carbon Mater.*, 2009, **24**, 301–306.

32 Y. Zhang, H. Ma, K. Zhang, S. Zhang and J. Wang, An improved DNA biosensor built by layer-by-layer covalent attachment of multi-walled carbon nanotubes and gold nanoparticles, *Electrochim. Acta*, 2009, **54**, 2385–2391.

33 V. Fierro, V. Torné-Fernández, D. Montané and A. Celzard, Adsorption of phenol onto activated carbons having different textural and surface properties, *Microporous Mesoporous Mater.*, 2008, **111**, 276–284.

34 M. Mermoux, Y. Chabre and A. Rousseau, *Carbon*, 1991, **29**, 469.

35 W. W. Cai, R. D. Piner, F. J. Stadermann, S. Park, M. A. Shaibat, Y. Ishii, D. X. Yang, A. Velamakanni, S. J. An, M. Stoller, J. H. An, D. M. Chen and R. S. Ruoff, *Science*, 2008, **321**, 1815.

36 L. Verbit, *J. Am. Chem. Soc.*, 1965, **87**, 1617.

37 H. Hosoya, J. Tanaka and S. Nagakura, *J. Mol. Spectrosc.*, 1962, **8**, 257.

38 O. Akhavan and E. Ghaderi, *J. Phys. Chem. C*, 2009, **113**, 20214.

39 Q. Lai, S. Zhu, X. Luo, M. Zou and S. Huang, Ultraviolet-visible spectroscopy of graphene oxides, *AIP Adv.*, 2012, **2**, 032146.

40 O. Akhavan and E. Ghaderi, *J. Chem. Phys. C*, 2009, **113**, 20214.

41 Y. H. Wang, L. L. Li, C. N. Luo, X. J. Wang and H. M. Duan, Removal of Pb^{2+} from water environment using a novel magnetic chitosan/graphene oxide imprinted Pb^{2+}, *Int. J. Biol. Macromol.*, 2016, **86**, 505–511.

42 Z. Lin, X. Weng, L. Ma, B. Sarkar and Z. Chen, Mechanistic insights into Pb(II) removal from aqueous solution by green reduced graphene oxide, *J. Colloid Interface Sci.*, 2019, **550**, 1–9.

43 N. H. Kim, T. Kuila and J. H. Lee, Simultaneous reduction, functionalization and stitching of graphene oxide with ethylenediamine for composites application, *J. Mater. Chem. A*, 2013, **1**, 1349.

44 O. K. Park, M. G. Hahm, S. Lee, H. I. Joh, S. I. Na, R. Vajtai, J. H. Lee, B. C. Ku and P. M. Ajayan, In situ synthesis of thermochemically reduced graphene oxide conducting nanocomposites, *Nano Lett.*, 2012, **12**, 1789.

45 A. C. Ferrari, J. C. Meyer, V. Scardaci, C. Casiraghi, M. Lazzeri, F. Mauri, S. Piscanec, D. Jiang, K. S. Novoselov, S. Roth and A. K. Geim, *Phys. Rev. Lett.*, 2006, **97**, 187401.

46 K. S. Rao, J. Senthilnathan, Y.-F. Liu and M. Yoshimura, Role of Peroxide Ions in Formation of Graphene Nanosheets by Electrochemical Exfoliation of Graphite, *Sci. Rep.*, 2014, **4**, 4237.

47 T. Lin, J. Chen, H. Bi, D. Wan, F. Huang, X. Xie and M. Jiang, *J. Mater. Chem. A*, 2013, **1**, 500.

48 F. Zeng, Z. Sun, X. Sang, D. Diamond, K. T. Lau, X. Liu and D. S. Su, *ChemSusChem*, 2011, **4**, 1587.

49 M. Strankowski, D. WBodarczyk, A. Piszczyk and J. Strankowska, Polyurethane Nanocomposites Containing Reduced Graphene Oxide, FTIR, Raman, and XRD Studies, *J. Spectrosc.*, 2016, 7520741, 6 pages.

50 T. Guo, C. Bulin, Bo Li, Z. Zhao, H. Yu, S. He, X. Ge, R. Xing and B. Zhang, Efficient removal of aqueous Pb(II) using partially reduced graphene oxide-Fe3O4, *Adsorpt. Sci. Technol.*, 2018, **36**(3–4), 1031–1048.

51 Y. Xu, H. Bai, G. Lu, C. Li and G. Shi, Flexible graphene films via the filtration of water-soluble noncovalent functionalized graphene sheets, *J. Am. Chem. Soc.*, 2008, **130**, 5856–5857.

52 L. Liu, S. X. Liu, Q. P. Zhang, C. Li, C. L. Bao, X. T. Liu and P. F. Xiao, Adsorption of Au(III), Pd(II), and Pt(IV) from aqueous solution onto graphene oxide, *J. Chem. Eng. Data*, 2012, **58**, 209–216.

53 M. Osińska, Removal of lead(II), copper(II), cobalt(II) and nickel(II) ions from aqueous solutions using carbon gels, *J. Sol-Gel Sci. Technol.*, 2017, **81**, 678–692.

54 A. K. Meena, G. K. Mishra, P. K. Rai, C. Rajagopal and P. N. Nagar, Removal of heavy metal ions from aqueous solutions using carbon aerogels as an adsorbent, *J. Hazard. Mater. B*, 2005, **122**, 161–170.

55 Y. Xue, H. Hou and S. Zhu, Competitive adsorption of copper(II), cadmium(II), lead(II) and zinc(II) onto basic oxygen furnace slag, *J. Hazard. Mater.*, 2009, **162**, 391–401.

56 M. Yari, M. Norouzi, A. H. Mahvi, M. Rajabi, Y. Ali, O. Moradi, I. Tyagi and V. K. Gupta, Removal of Pb(II) ion from aqueous solution by graphene oxide and functionalized graphene oxide-thiol: effect of cysteamine concentration on the bonding constant, *Desalin. Water Treat.*, 2016, **57**, 11195–11210.

57 C. Gao, Z. Dong, X. Hao, Y. Yao and S. Guo, Preparation of Reduced Graphene Oxide Aerogel and Its Adsorption for Pb(II), *ACS Omega*, 2020, **5**, 9903–9911.

58 N. N. Nassar, Rapid removal and recovery of Pb(II) from wastewater by magnetic nanoadsorbents, *J. Hazard. Mater.*, 2010, **184**(1–3), 538–546.

59 G. Annadurai, R. S. Juang and D. J. Lee, Adsorption of rhodamine 6G from aqueous solutions on activated carbon, *J. Environ. Sci. Health, Part A: Toxic/Hazard. Subst. Environ. Eng.*, 2001, **36**(5), 715–725.

60 Van H. Nguyen, H. T. Van, Van Q. Nguyen, X. Van Dam, L. P. Hoang and L. T. Ha, Magnetic Fe_3O_4 Nanoparticle Biochar Derived from Pomelo Peel for Reactive Red 21 Adsorption from Aqueous Solution, *J. Chem.*, 2020, 3080612, 14 pages.

61 L. Pan, Z. Wang, Y. Qi and R. Huang, Efficient Removal of Lead, Copper and Cadmium Ions from Water by a Porous Calcium Alginate/Graphene Oxide Composite Aerogel, *Nanomaterials*, 2018, **8**, 957.

62 G. Zhao, X. Ren, X. Gao, X. Tan, J. Li, C. Chen, Y. Huang and X. Wang, Removal of Pb(II) ions from aqueous solutions on few-layered graphene oxide nanosheets, *Dalton Trans.*, 2011, **40**, 10945.

63 K. X. Zhang, H. Y. Li, X. J. Xu and H. W. Yu, Synthesis of reduced graphene oxide/NiO nanocomposites for the removal of Cr (VI) from aqueous water by adsorption, *Microporous Mesoporous Mater.*, 2018, **255**, 7–14.

64 Y. L. F. Musico, C. M. Santos, M. L. P. Dalidab and D. F. Rodrigues, Improved removal of lead(II) from water using a polymer-based graphene oxide nanocomposite, *J. Mater. Chem. A*, 2013, **1**, 3789–3796.

65 S. Pourbeyram, Effective Removal of Heavy Metals from Aqueous Solutions by Graphene Oxide–Zirconium Phosphate (GO–Zr-P) Nanocomposite, *Ind. Eng. Chem. Res.*, 2016, **55**(19), 5608–5617.

66 L. P. Lingamdinne, J. R. Koduru, Y.-Y. Chang and R. R. Karri, Process optimization and adsorption modeling of Pb(II) on nickel ferrite–reduced graphene oxide nano-composite, *J. Mol. Liq.*, 2018, **250**, 202–211.

67 S. Ahmad, A. Ahmad, S. Khan, S. Ahmad, I. Khan, S. Zada and P. Fu, Algal extracts based biogenic synthesis of reduced graphene oxides (rGO) with enhanced heavy metals adsorption capability, *J. Ind. Eng. Chem.*, 2019, **72**, 117–124.

68 N. S. Tabrizi and S. Zamani, Removal of Pb(II) from aqueous solutions by graphene oxide aerogels, *Water Sci. Technol.*, 2016, **74**(1), 256–265.

69 Y. Q. He, N. N. Zhang and X. D. Wang, Adsorption of graphene oxide/chitosan porous materials for metal ions, *Chin. Chem. Lett.*, 2011, **22**(7), 859–862.

70 G. D. Vukovic, A. D. Marinkovic, S. D. Skapin, M. Ristic, R. Aleksic, A. Peric-Grujic and P. S. Uskokovic, Removal of lead from water by amino modified multi-walled carbon nanotubes, *Chem. Eng. J.*, 2011, **173**, 855–865.

71 O. Moradi, K. Zare, M. Monajjemi, M. Yari and H. Aghaie, The studies of equilibrium and thermodynamic adsorption

of Pb(II), Cd(II) and Cu(II) Ions from aqueous solution onto SWCNTs and SWCNT–COOH surfaces, *Fullerenes, Nanotubes, Carbon Nanostruct.*, 2010, **18**, 285–302.

72 X. Ao and H. Guan, Preparation of Pb(II) ion-imprinted polymers and their application in selective removal from wastewater, *Adsorpt. Sci. Technol.*, 2018, **36**(1–2), 774–787.

73 W. Peng, G. Han, Y. Cao, K. Sun and S. Song, Efficiently Removing Pb(II) from Wastewater by Graphene Oxide using Foam Flotation, *Colloids Surf., A*, 2018, **556**, 266–272.

74 B. Wei, X. Cheng, G. Wang, H. Li, X. Song and D. Liang, Graphene Oxide Adsorption Enhanced by Attapulgite to Remove Pb (II) from Aqueous Solution, *Appl. Sci.*, 2019, **9**, 1390.

75 J. Shen, M. Zhang, G. Liu, K. Guan and W. Jin, Size effects of graphene oxide on mixed matrix membranes for CO_2 separation, *AIChE J.*, 2016, **62**, 2843–2852.

76 N. Zhang, P. Qi, Y. H. Ding, C. J. Huang, J. Y. Zhang and Y. Z. Fang, A novel reduction synthesis of the graphene/Mn3O4 nanocomposite for supercapacitors, *J. Solid State Chem.*, 2016, **237**, 378–384.

77 G. Shao, Y. Lu, C. Yang, F. Zeng and Q. Wu, Graphene oxide: the mechanisms of oxidation and exfoliation, *J. Mater. Sci.*, 2012, **47**, 4400–4409.

78 J. Wang, Y. Li, Z. Lv, Y. Xie, J. Shu, A. Ahmed, T. Hayat and C. Chen, Exploration of the adsorption performance and mechanism of zeolitic imidazolate framework-8@graphene oxide for Pb(II) and 1-naphthylamine from aqueous solution, *J. Colloid Interface Sci.*, 2019, **542**, 410–420.

79 W. Peng, H. Li, Y. Liu and S. Song, Comparison of Pb(II) adsorption onto graphene oxide prepared from natural graphites: Diagramming the Pb(II) adsorption sites, *Appl. Surf. Sci.*, 2016, **364**, 620–627.

80 P. Y. Shih, J. Y. Ding and S. Y. Lee, MAS-NMR and FTIR analyses on the structure of CuO-containing sodium poly- and meta-phosphate glasses, *Mater. Chem. Phys.*, 2003, **80**, 391–396.

81 R. Han, Z. Lu, W. Zou, W. Daotong, J. Shi and Y. Jiujun, Removal of copper(II) and lead(II) from aqueous solution by manganese oxide coated sand II. Equilibrium study and competitive adsorption, *J. Hazard. Mater.*, 2006, **137**, 480–488.

82 D. Xu, X. Tan, C. Chen and X. Wang, Removal of Pb(II) from aqueous solution by oxidized multiwalled carbon nanotubes, *J. Hazard. Mater.*, 2008, **154**, 407–416.

83 C. J. Madadrang, H. Y. Kim, G. Gao, N. Wang, J. Zhu, H. Feng, M. Gorring, M. L. Kasner and S. Hou, Adsorption behavior of EDTA-graphene oxide for Pb(II) removal, *ACS Appl. Mater. Interfaces*, 2012, **4**, 1186–1193.